2.3

TWO-DIMENSIONAL IDEALIZED SIMULATIONS OF THE IMPACT OF MULTIPLE WINDWARD RIDGES ON OROGRAPHIC PRECIPITATION

Brian A. Colle

Institute for Terrestrial and Planetary Atmospheres, Stony Brook University / SUNY, Stony Brook, NY

1. INTRODUCTION

The impact of terrain-induced gravity waves (mountain waves) on orographic precipitation has received increased attention lately, since it has been shown using both observations and numerical models that these waves can have a profound impact on the precipitation distribution. For example, Garvert et al. (2005; 2006) used in situ aircraft and radar observations to show the enhancement in vertical motion and precipitation by gravity waves over the narrow ridges of the windward Oregon Cascades. Meanwhile, Colle (2004) used two-dimensional simulations to show that the upstream vertical tilt of a mountain wave over the crest can displace the precipitation 50-100 km upstream of the crest for a relatively wide (50-km half width) barrier under stabily-stratified conditions. Smith and Barstad (2004) developed a linear theory of stable orographic precipitation, which included analytical solutions to the mountain wave problem for different terrain geometries and appropriate cloud process timescales.

Narrow windward ridges can enhance the precipitation locally over the ridge, but can a series of windward ridges increase the net precipitation along the windward slope? The answer is not obvious, since downwind of each ridge the precipitation may be reduced because of downslope drying and removal of water vapor over the previous ridge. Garvert et al. (2006) began to address this question by replacing the real Cascade terrain in the MM5 with a smooth slope, while preserving the mean height of the Cascade crest. They showed for the 13-14 December IMPROVE-2 event that the total windward precipitation at the surface was enhanced by 10-20%. Therefore, this suggests that the precipitation efficiency over a relatively wide barrier such as the Cascades can be enhanced when there are a series of ridges rather than a smooth slope.

More case studies are needed to further quantify the results of Garvert et al. (2006) for other synoptic settings and barrier dimensions. Meanwhile, additional motivation for these case studies may be obtained by completing a range of idealized studies. Therefore, the goal of this study is to extend their results using two-dimensional idealized MM5 simulations. This study will address the following motivational questions:

- What is the impact of multiple ridges on the precipitation structures over a relatively wide barrier?
- How do the ridges affect the drying ratio and microphysical time scales?
- How do the ridge impacts change for different flow speeds, stabilities, and freezing levels?

2. DATA AND METHODS

This study follows Colle (2004), in which the MM5 was used in a two-dimensional configuration for a 1500 grid point domain with 1-km horizontal grid spacing, 38 vertical half sigma levels, and constant (fixed) lateral boundary conditions. The large size of this domain prevented any spurious reflections from the boundaries from affecting the terrain flows near the center of the domain. Although a two-dimensional model has some limitations, it was more feasible to use than a large three-dimensional domain given the hundreds of simulations that were completed.

In order to relate the idealized results to a relatively wide and high barrier such as the Cascades, the MM5 simulations in this study used a bell-shaped mountain ridge height (h_m) of 2000 m and a half width (a) of 50 km located in the middle of the domain. The terrain height, h(x),

$$h = \frac{h_m}{(\frac{x}{a})^2 + 1} + h' \sin(2\pi n x / L); \quad \text{for } x = 0 \text{ to } -L \qquad (1)$$

and

$$h = \frac{h_m}{(\frac{x}{a})^2 + 1}; \quad \text{for } x > 0 \text{ and } x < -L, \qquad (2)$$

included sinusoidal height perturbations (h') for *n* number of windward ridges superimposed from the crest (x = 0) to –L upstream (Fig. 1), which for this study was –3a (150 km). With this terrain perturbation approach the average terrain height of the barrier does not change. The 50-km half width and 2000 m mountain height used in this study is similar to a relatively wide barrier, such as the Oregon Cascades and California Sierras. The height perturbation (h') was varied from 200, 400, and 800 m for *n* = 0, 1, 2, 4, 6, 8, 10, 12, 14, and 16.

The model was initialized as nearly saturated (98% relative humidity); therefore, a moist static stability (N_m) of 0.005 s^{-1} and 0.01 s^{-1} was utlized, with the weaker stability close to the low-level conditions observed during 13-14 December 2001 of IMPROVE-2 (Garvert et al. 2005). Both the different stratifications and variations in cross barrier ambient flow (U) from 8, 15, and 30 m s^{-1} helped control the amount of flow blocking and gravity wave structure above the barrier. Freezing levels (FLs) were specified to be either at 1000, 750, and 500 mb. As noted in Colle (2004), the precipitation amounts for the different N_m and FL settings cannot be compared quantitatively, since they have different integrated water amounts; however, the structure of the precipitation distribution and microphysical efficiencies can still be analyzed.

**Corresponding author address:* Dr. Brian A. Colle, Marine Sciences Research Center, Stony Brook University/SUNY, Stony Brook, NY 11794-5000. email: brian.colle@stonybrook.edu

The MM5 was integrated for 12 h using the Thompson et al. (2004) microphysical scheme. This scheme includes six water species: water vapor, cloud water, cloud ice, snow, and graupel. The medium-range forecast (MRF) planetary boundary layer scheme was applied using a surface roughness length z_o of 10 cm; however, no surface heat/moisture fluxes and radiation were included. Both Rayleigh damping and Klemp and Durran's (1983) upper-radiative boundary condition were used at the upper boundary to prevent gravity wave reflection. As described in Colle (2004), the 2-D MM5 included the Coriolis effect for a representative midlatitude value of $f \sim 10^{-4}$ s^{-1}.

A few quantities were calculated to better understand the precipitation generation and microphysical time scales. A drying ratio (DR) measures the ratio of precipitation to the incoming flux of water vapor (Smith et al. 2003). The DR was calculated by comparing the total surface precipitation accumulated over the barrier (–3a upstream of crest to 1a in lee) to the water vapor flux entering the region. Another way to quantify microphysical efficiency is determining the characteristic time for all water and ice generated aloft to fall as precipitation. This residence time (RT) is defined as the total condensation and deposition rate divided by the precipitation rate.

3. RESULTS

The first series of ridge experiments used an N_m of 0.005 s^{-1}, U of 8, 15, and 30 m s^{-1} (U8, U15, and U30), a freezing level of 750 mb, and ridge height perturbation of 400 m. Figures 1a,b shows some terrain and 6-12h precipitation profiles for a few select ridge numbers and U15. For the n = 0 run (Fig. 1b), the maximum precipitation (26 mm) was located about 25 km upstream of the crest, with precipitation decreasing exponentially upstream to the bottom of the lower windward slope. For n = 4, the maximum precipitation near the crest is 40% greater than n = 0. For each subsequent ridge along the windward slope for n = 4, the precipitation amount increases nearly steadily from 22 mm at ~5 km upstream of first peak to 43 mm at ~5 km downwind of the final windward peak, while the precipitation is less than 5 mm within the windward valleys. For n = 8 (not shown), the greatest precipitation over the lower windward slope (~30 mm) is located over the second peak, and there is a slight decrease in the precipitation maxima over the next two subsequent ridges along the windward slope, followed by a spike to 40 mm over the final windward ridge. For n =12 and n =16 (Fig. 1b), the precipitation also maximizes over the second ridge and just upwind of the crest. Interestingly, the precipitation maxima over the windward ridges for n =12 are greater than n =16, suggesting that the n = 16 ridges are too narrow to efficiently remove precipitation as compared to n =12. There is also an interesting transition ~35 km upstream of the crest, where there is much less precipitation variability between the ridges and valleys, which transitions to larger precipitation variability near the crest.

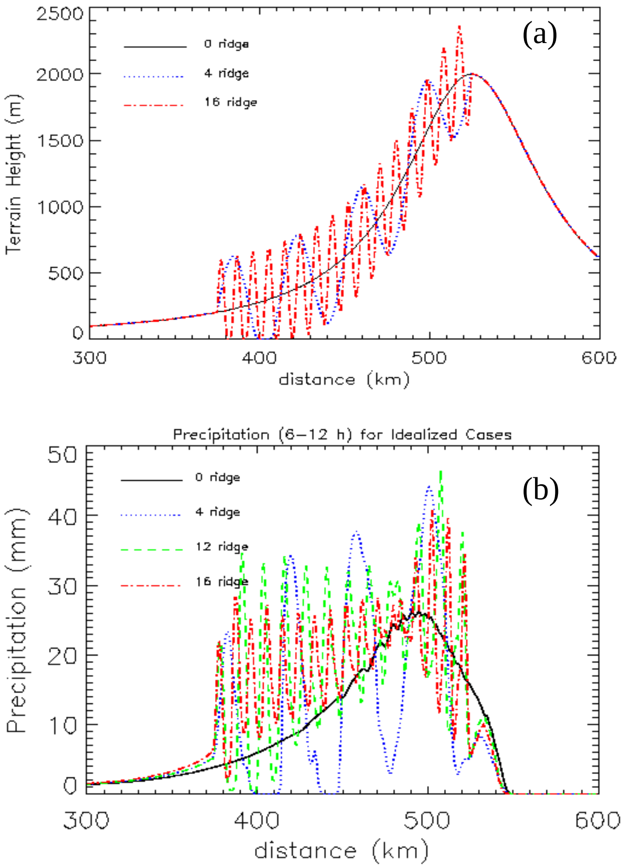

Figure 1. (a) Terrain (in meters) for a few select windward ridge numbers (n = 0, 4, and 16) used in the idealized experiments. (b) Precipitation (in mm) across the barrier between hours 6 and 12 of n = 0, 4, 12, and 16 simulations.

Figure 2 shows the cross section of winds and precipitation hydrometeors for many of the above simulations. For n = 0 (Fig. 2a), there is a broad orographic snow cloud aloft associated with a single linear mountain wave tilting upstream of the crest, while graupel exists over the upper windward slope. With the addition of a single ridge upstream of the crest (n = 1; not shown), the vertical motion with upstream gravity wave results in a snow plume aloft (0.22 g kg^{-1}) of similar magnitude to the snow aloft near the crest, even though the crest is 1500 m higher. The slope near the crest is steeper and higher, so there is more graupel and larger rain rates near the crest. For n = 4 (Fig. 2c), the graupel amount increases over each subsequent ridge towards the crest as the windward slopes get steeper and higher toward the crest, while there is less percentage increase of snow towards the crest. As n increases to 12 (Fig. 2c), there are less pronounced localized snow maxima over the individual ridges aloft, as snow is advected more from one ridge to another, rather than sublimating in between. Meanwhile, the graupel plumes are still prevalent over the individual ridges for n = 12. These graupel plumes are weaker over the lower windward slopes for n = 16 (Fig. 2d), and the snow is less perturbed aloft. For both n = 12 and 16, there is strong subsidence near the crest of the barrier, which is advecting hydrometeors in the surface, thus creating the localized precipitation maximum in that region (Fig. 2b).

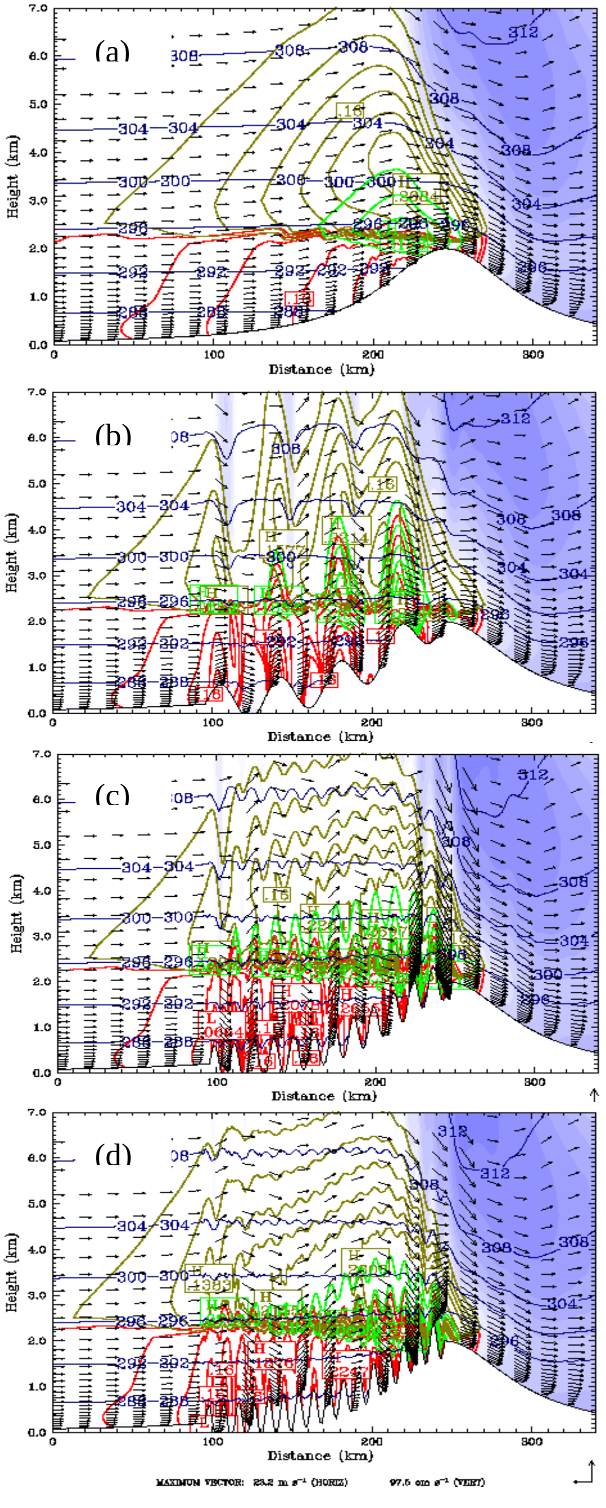

Figure 2. Cross section of potential temperature (every 4 K), wind circulation vectors (see scale in d), snow (yellow every 0.04 g kg^{-1}), graupel (green every 0.08 g kg^{-1}), and rain (red every 0.04 g kg^{-1}) mixing ratios averaged for hours 6-12 for the (a) n = 0, (b) n = 4, (c) n =12, and (d) n =16 windward ridge experiments using U = 15 m s^{-1} and N_m = 0.005 s^{-1}.

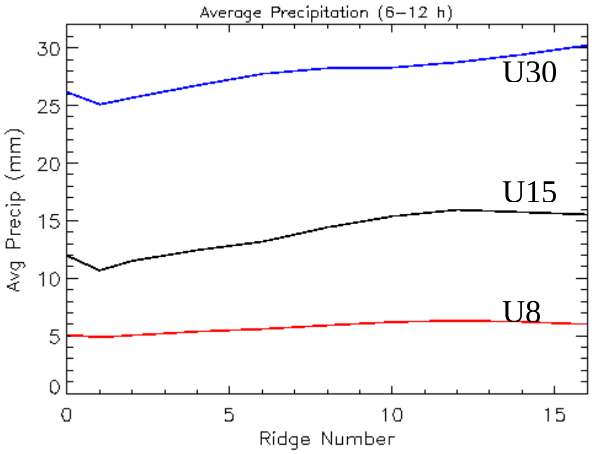

Figure 3. Surface precipitation (in mm) between hours 6-12 averaged over the windward slope as a function of ridge number for the U = 8 m s^{-1} (red), 15 m s^{-1} (black), and 30 m s^{-1} (blue) experiments using N_m = 0.005 s^{-1}.

Figure 3 shows the average 6-12 h surface precipitation between 1a (50 km) downwind of the crest to 3a (150 km) upstream of the crest for the U8, U15, and U30 runs. For U15, there is an initial decrease from 12 to 10 mm from n = 0 to 1 associated with the large area of lee side subsidence downwind of the first windward ridge. Subsequently, the average windward precipitation increases nearly linearly from 10 for n =2 to 15 mm for n = 12, followed by a slight decrease for n > 12. The drying ratio (DR) for this same region shows an increase from 0.32 for n =1 to 0.46 for n =12 (Fig. 5b). Therefore, the addition of the ridges increase of the efficiency at which water vapor is removed, which increases the net precipitation by ~30% for n = 12. For U8 there is an 18% increase in precipitation (5 to 6 mm) and a DR increase of 0.30 to 0.37 for n = 1 to 12. For U30, the average precipitation increase occurs from n = 1 to 8 and n > 12, and the DR increases from 0.37 to 0.41 at n = 1 to 12, respectively. The relatively strong cross-barrier flow in U30 does not allow hydrometeors time to grow and fallout as efficiently for increasing n as compared to U15, with the U15 runs having a larger DR for n =12 (not shown).

The maximum precipitation and location along the windward slope was also quantified for various ridges numbers and wind speeds (not shown). For U15, the maximum precipitation has a peak of ~45 mm at n =4 and n = 12. The first maximum is located ~25 km upward of the crest, while the second maximum is ~15 km upwind. Meanwhile, the maximum precipitation for U8 occurs for n = 4 at ~30 km upwind of the crest. For n > 4, the maximum precipitation decreases and is located ~50 and 25 km upwind of the crest for n = 12 and n = 16, respectively. In contrast, for U30, the maximum precipitation increases nearly linearly from ~60 mm at n =2 to ~72 mm at n =10 and the precipitation maximum shifts towards the crest from ~60 km upwind at n =2 to ~5 km upwind at n = 10.

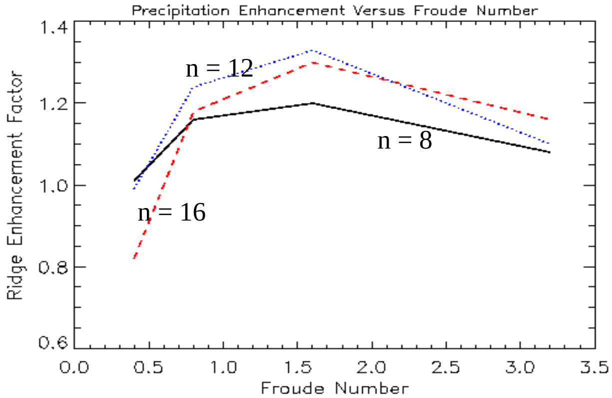

Figure 4. The fractional enhancement of precipitation above the no windward ridge run (n =0) for the n = 8, 12, and 16 versus the Froude number.

Additional simulations were completed using a greater stability (N_m = 0.01 s^{-1}) in order to create a regime diagram of the fractional enhancement of precipitation, as measured relative to the no windward ridge run (n = 0), versus Froude number, $U/(h_m N_m)$ (Fig. 4). For n = 8, 12, and 16, the multiple ridges result in no average precipitation enhancement for relatively low Froude numbers (Fr ~0.4). Under these conditions the flow is nearly stagnated at the surface over the lower barrier slope and windward valleys (Fig. 5). The weaker flow favors weaker vertical motions over the barrier (0.5 m s^{-1} as compared to ~1 m s^{-1} in Fig. 3) and less snow aloft. The shallow vertical wavelength of the gravity wave over the barrier ($2\pi U/N_m$ ~6500 m) also yields a shallow snow area; thus, the ridge effects on precipitation are limited to below 3-km ASL. The enhancement of the each ridge is offset by the minimum in the valley, thus resulting in little average enhancement by the ridges over the windward slope. For moderate Froude numbers (0.8-1.5), there are more well-defined mountain waves and vertical motions over the barrier (Fig. 3), thus resulting is 20-30% average enhancement for n > 8. When the Froude number is increased to 3.0, the ridge enhancement decreases to < 20% as the mountain wave amplitude decreases (not shown), and the stronger cross barrier flow favors less time for precipitation growth over the ridge before advecting into the valley.

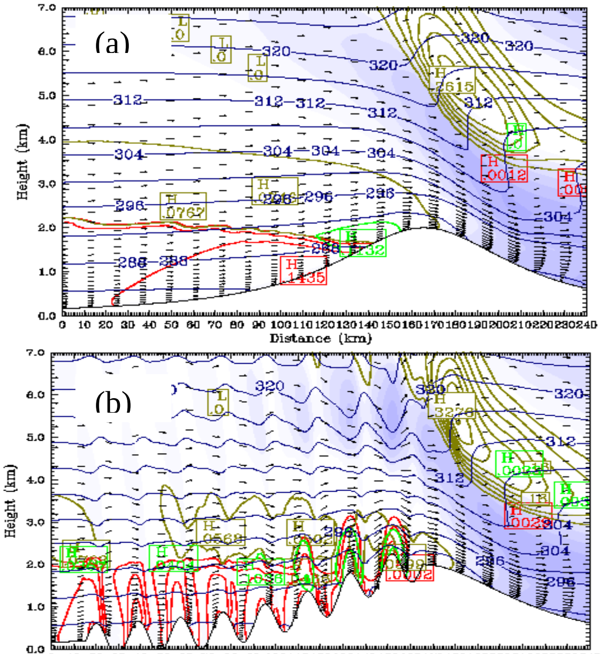

Figure 5. Same as Fig. 3 except for N = 0.01 s^{-1} and U = 8 m s^{-1} showing (a) n = 0 and (b) n = 8.

Additional simulations using U = 15 m s^{-1} and N = 0.005 s^{-1} were completed, in which the freezing level (FL) was raised to 500 mb and lowered to 1000 mb. For all freezing levels (Fig. 6), the maximum ridge precipitation enhancement averaged over the barrier is for n = 12. The 25-30% average precipitation enhancement for the 500-mb FL is similar to the 750-mb. However, for the 1000-mb FL, the average ridge enhancement is only ~15% by n = 12. The 1000-mb had much less graupel growth over the ridges (not shown), thus limiting the precipitation enhancement.

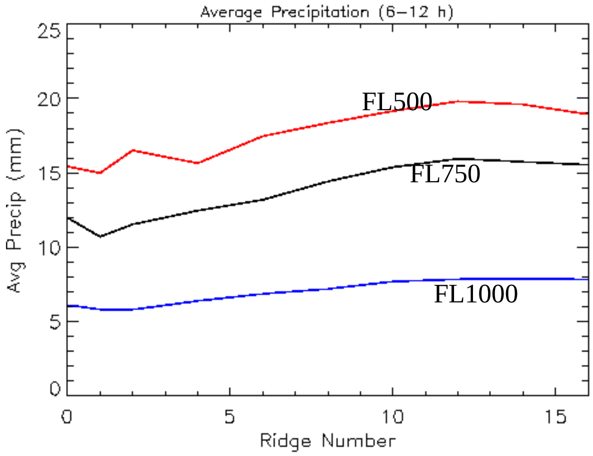

Figure 6. Surface precipitation (in mm) between hours 6-12 averaged over the windward slope as a function of ridge number for the freezing level (FL) = 500 mb (red), 750 mb (black), and 1000 mb (blue) using N_m = 0.005 s^{-1} and U = 15 m s^{-1}.

In order to test the impact of the height of the windward ridges, their amplitude (h’) was varied from 200 to 800 m for N = 0.005 s^{-1}, U = 15 m s^{-1}, and FL = 750 mb. For n = 1 and 2 (Fig. 7), there is little difference in average precipitation over the windward slope for various windward ridge heights. For small n, as h’ is increased to 800 m the precipitation increases over the ridges (not shown), however, the amount of subsidence drying also increases over the subsequent valleys. Thus, for small n there is little net gain of average precipitation over the windward slope. As n is increased from 4 to 12, the average precipitation over the windward slope increases more dramatically for h’ = 800 m, reaching a maximum difference at n = 12. In general, the ridge heights have a more dramatic impact on average precipitation as n increases, with the steeper slopes of h’ = 800 m enhancing the multiple ridge impacts for larger n. However, even a series of h’ = 200 m ridges can have a 10-15% average enhancement in precipitation over the windward slope.

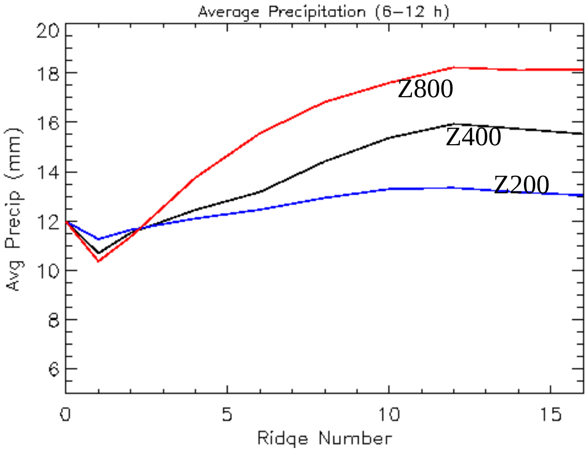

Figure 7. Same as Fig. 6 except for the windward ridge height perturbation (h') of 800 m (red), 400 m (black), and 200 m (blue) using $N_m = 0.005\ s^{-1}$, $U = 15\ m\ s^{-1}$, and FL = 750 mb.

4. CONCLUSIONS

This paper explored the impact of multiple ridges along a broad windward slope on the flow and precipitation structures. This was accomplished by completing many idealized two-dimensional simulations using MM5 for different stabilities, flow speeds, ridge numbers (n), and freezing levels. In agreement with a recent case study from IMPROVE-2 (Garvert et al. 2006), relatively small ridges (200-400 m) can have a profound impact on the precipitation distribution over the barrier. This precipitation impact is strongly dependent on the number of ridges over the barrier, with fewer ridge numbers (n < 4) favoring larger precipitation perturbations over the individual ridges, while greater ridge numbers (n > 8) favor a 15-30% increase in average precipitation over the windward slope. For light to moderate wind speeds (U ~ 8 and 15 m s^{-1}), the multiple ridge impact on average precipitation peak for n = 12 (ridge-valley wavelenth of 12.5 km), while the enhancement continues to increase for from n = 12 to n = 16 for U = 30 m s^{-1}.

For Froude numbers << 1, the ridges do not increase the average precipitation over the windward slope. Some of this is attributed to shallow flow blocking, and the weaker flow also favors a shallower orographic cloud given the smaller vertical gravity wavelength over the barrier. Large Froude numbers (Fr >> 1) also have more limited ridge effects, since the stronger flow results in a more evanescent wave response aloft and less time for precipitation growth over the individual ridges.

A higher freezing level (FL of 750 to 500 mb) favors large precipitation perturbations over the individual ridges because of enhanced riming and accretional processes. The enhancement in average precipitation over the windward slope is similar for a FL of 500 and 750 mb. In contrast, a lower FL (1000 mb) has less ridge impacts, since there is less riming aloft.

The windward precipitation is also sensitive to the height of the ridge perturbations (h'). For small n (n < 4), the average precipitation over the windward slope does not increase with increasing h' from 200 to 800 m. As n increased from 4 to 12, the average precipitation over the windward slope increases more dramatically for h' = 800 m, reaching a maximum difference at n =12.

Future work will need to extend these idealized results to three dimensions as well as explore the impact of gravity waves on windward precipitation in field datasets such as IMPROVE-2.

5. ACKNOWLEDGEMENTS

This work was sponsored by the National Science Foundation (ATM-0450444).

6. REFERENCES

Colle, B. A., 2004: Sensitivity of orographic precipitation to changing ambient conditions and terrain geometries: An idealized modeling perspective. *J. Atmos. Sci.*, **61**, 588-606.

Garvert, M., B. A. Colle, and C. F. Mass, 2005: The 13-14 December IMPROVE event: Part I, Synoptic and mesoscale comparison of the observed structures with a mesoscale model simulation. *J. Atmos. Sci.*, **62**, 3474-3492.

__________, B. F. Smull, and C.F. Mass, 2006: Mountain wave structure occurring within an orographic precipitation event. Submitted to *J. Atmos. Sci.*

Klemp, J. B., and D. R. Durran, 1983: An upper boundary condition permitting internal gravity wave radiation in numerical mesoscale models. *Mon. Wea. Rev.*, **111**, 430–444.

Smith, R. B., and Barstad, I., 2004: A linear theory of orographic precipitation. *J. Atmos. Sci.*, **61**, 1377-1391.

__________, Q. Jiang, M. Fearon, P. Tabary, M. Doringer, J. Doyle, and R. Benoit, 2003: Orographic precipitation and airmass transformation: An Alpine example. *Quart. J. Roy. Meteor. Soc.*, **129**, 433-454.

Thompson, G., R. M. Rasmussen, and K. Manning, 2004: Explicit forecasts of winter precipitation using an improved bulk microphysics scheme. PartI: Description and sensitivity analysis. *Mon. Wea. Rev.*, **132**, 519–542.